The Astronomical Journal, 151:143 (7pp), 2016 June doi:10.3847/0004-6256/151/6/143

SILICON DEPLETION IN THE INTERSTELLAR MEDIUM

U. Haris[1], V. S. Parvathi[2], S. B. Gudennavar[1], S. G. Bubbly[1], J. Murthy[3], and U. J. Sofia[4]
[1] Department of Physics, Christ University, Hosur Road, Bangalore, Karnataka 560029, India; haris380@gmail.com, shivappa.b.gudennavar@christuniversity.in, bubbly.sg@christuniversity.in
[2] Department of Physics, St. Joseph's College (Autonomous), Lalbagh Road, Bangalore-560027, India; veena.makesh@gmail.com
[3] Indian Institute of Astrophysics, II Block, Koramangala, Bangalore 560034, India; jmurthy@yahoo.com
[4] Department of Physics, American University, 4400 Massachusetts Avenue, NW, Washington, DC 20016, USA; sofia@american.edu
Received 2014 February 16; accepted 2016 March 15; published 2016 May 18

ABSTRACT

We report interstellar silicon (Si) depletion and dust-phase column densities of Si along 131 Galactic sight lines using archival observations. The data were corrected for differences in the assumed oscillator strength. This is a much larger sample than previous studies but confirms the majority of results, which state that the depletion of Si is correlated with the average density of hydrogen along the line of sight ($\langle n(\mathrm{H})\rangle$) as well as the fraction of hydrogen in molecular form ($f(\mathrm{H_2})$). We also find that the linear part of the extinction curve is independent of Si depletion. Si depletion is correlated with the bump strength (c_3/R_V) and the FUV curvature (c_4/R_V) suggesting that silicon plays a significant role in both the 2175 Å bump and the FUV rise.

Key words: dust, extinction – ISM: abundances

Supporting material: machine-readable tables

1. INTRODUCTION

Depletion studies, particularly those of highly abundant species, are one way to understand the chemical composition of the interstellar medium (ISM) and of interstellar dust grains. One of the most important components of interstellar dust is silicon, which has a high condensation temperature (1346 K) and is one of the most abundant metals in the universe (Lodders et al. 2009). Si is also particularly interesting because it shows a wide range of depletions in neutral clouds unlike other abundant elements such as Fe, O, and C. It may comprise up to 70% of the core mass of the dust grains (Weingartner & Draine 2001) in the form of silicates. These may be formed in the outflows of oxygen-rich asymptotic giant branch stars, red supergiants, and supernovae (Tielens 2005) and are then processed in the diffuse ISM (Henning 2010). A study of their abundances over a number of different lines of sight will help us understand the composition and processing of dust grains in different environments.

We have used a compilation of interstellar column densities by Gudennavar et al. (2012) to trace the distribution of silicon and the variation of the dust properties with the silicon abundance. The properties and the amount of interstellar dust vary considerably over these sight lines with $E(B-V)$ ranging from 0.01 to 0.78 and $R_V(=A_V/E(B-V))$ ranging from 2.02 to 5.84. The sheer number of observations help to clarify correlations and relationships suggested by smaller studies, and we plan to use these data to study other interrelationships between elements in the ISM.

Details of the data and analysis are given in Section 2. In Section 3 we have presented the results and discussion. In Section 4 we have summarized our conclusions.

2. DATA AND METHODOLOGY

Gudennavar et al. (2012) compiled absorption line data for 3008 stars of which 131 sight lines included silicon column densities that were taken over 30 years of observations (Table 1). Most of the sight lines are near the Galactic plane (Figure 1), and therefore sample dense regions with a complex structure.

There have been four methods used in the literature to derive column densities from the observed absorption lines: Curve Of Growth (COG), Apparent Optical Depth (AOD), Profile Fitting (PF), and Continuum Reconstruction. A brief explanation of these methods and a detailed description of the data is given in Gudennavar et al. (2012).

Most of the silicon lines (84) in our sample have come from van Steenberg & Shull (1988) who used archival observations from the *International Ultraviolet Explorer* (*IUE*) to derive column densities to a number of different species. Because of the relatively poor resolution and low signal-to-noise of *IUE*, van Steenberg and Shull fit the abundances with a COG. Most of the other observations (36) were made using the Goddard High Resolution Spectrograph (Spitzer & Fitzpatrick 1995; Savage & Sembach 1996; Redfield & Linsky 2004) or the Space Telescope Imaging Spectrograph (Sonnentrucker et al. 2003; Gnacinski & Krogulec 2006; Miller et al. 2007) with higher resolution and better signal-to-noise, which allowed for PF or, equivalently, AOD fitting. In all cases, the Si II lines are on the flat part of the COG (saturated in the case of strong lines) leading to a significant uncertainty in the derived column density.

The greatest source of error in the abundance measurements has been that the value of the oscillator strength of the lines has changed over the 30 years of observations. We have corrected all of the oscillator strengths to the latest values from the National Institute of Standards and Technology (NIST) (Kelleher & Podobedova 2008) and recalculated the column densities using the equation

$$\tau = 2.654 \times 10^{-2} N(X) f \phi(v), \quad (1)$$

where τ is the optical depth, $N(X)$ is the column density of the species in the cloud in units of atoms cm^{-2}, f is the oscillator strength of the transition, and $\phi(v)$ is the interstellar absorption profile. So long as $\tau \ll 1$, the equivalent width is commonly

Table 1
Sight Line Parameters and the Revised Column Densities of Silicon

Star Name	Galactic Coordinates[a]		Spectral type[a]	Distance[a]	$E(B-V)$ [a]	± Error[a]	$N(SiII)_{Revised}$ [b]	+Error[b]	−Error[b]
	l (deg)	b (deg)		(kpc)	(mag)		(cm^{-2})	(cm^{-2})	(cm^{-2})
HD 120315	100.70	65.32	B3V	0.03	0.08	0.01	8.90E+12	8.58E+11	−6.84E+11
HD 116658	316.11	50.84	B1III-IV+…	0.08	0.10	0.02	1.78E+13	1.39E+13	−1.39E+13
HD 158926	351.74	−2.21	B2IV+…	0.18	0.08	0.01	1.56E+14	4.10E+13	−4.10E+13
HD 122451	311.77	1.25	B1III	0.12	0.06	0.02	4.06E+14	9.46E+12	−9.25E+12
HD 064740	263.38	−11.19	B1.5Vp	0.23	0.01	0.01	4.45E+14	4.30E+13	−5.75E+13
HD 022928	150.28	−5.77	B5III	0.16	0.05	0.01	8.29E+14	5.93E+13	−7.30E+13
HD 023630	166.67	−23.46	B7III	0.12	0.05	0.01	8.44E+14	1.10E+13	−1.10E+13
HD 037742	206.45	−16.59	O9Iab:	0.05	0.13	0.01	1.07E+15	7.05E+14	−3.29E+14
HD 200120	88.03	0.97	B1.5Vnne	0.34	0.02	0.01	1.12E+15	7.38E+14	−3.96E+14
HD 093521	183.14	62.15	O9Vp	1.76	0.05	0.01	1.20E+15	2.79E+13	−8.00E+13
HD 157246	334.64	−11.48	B1Ib	0.35	0.05	0.01	1.38E+15	2.41E+14	−1.78E+14
HD 066811	255.98	−4.71	O4If(n)p	0.43	0.12	0.01	1.41E+15	4.91E+14	−1.24E+14
HD 036486	203.86	−17.74	O9.5II+…	0.21	0.08	0.01	1.19E+15	6.00E+13	−6.00E+13
HD 037043	209.52	−19.58	O9III	0.41	0.06	0.01	1.51E+15	1.46E+14	−1.64E+14
HD 038771	214.51	−18.50	B0Iab:	0.20	0.09	0.01	1.54E+15	3.60E+13	−3.73E+14

Notes.
[a] Gudennavar et al. (2012).
[b] Silicon column densities revised using the latest oscillator strengths taken from NIST (Kelleher & Podobedova 2008).
(This table is available in its entirety in machine-readable form.)

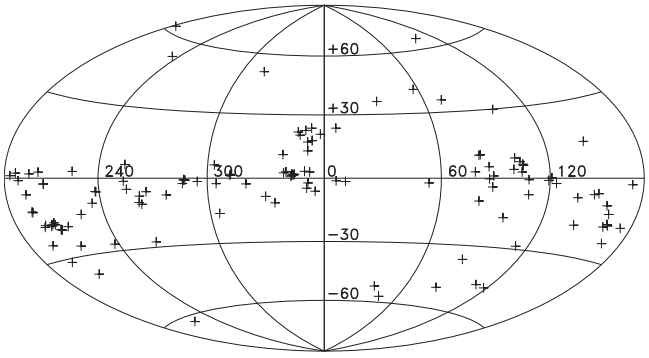

Figure 1. Distribution of stars in our data set plotted in an Aitoff plot with the Galactic center at the origin.

Table 2
Absorption Lines of Silicon

Vacuum Wavelength (Å)	f[a]
1020.6990	1.39E-02
1190.4158	2.77E-01
1193.2897	5.75E-01
1260.4221	1.22E+00
1304.3702	9.28E-02
1526.7066	1.33E-01
1808.0126	2.49E-03
2334.6050	2.99E-06

Note.
[a] Oscillator strength (f) values from the National Institute of Standards and Technology (NIST) (Kelleher & Podobedova 2008).

parameterized in terms of wavelength as

$$W/\lambda = 8.85 \times 10^{-13} N(X) f\lambda \qquad (.2)$$

Therefore, for a given transition with a certain value of equivalent width, the value of the column density will change with f. Considering this, we can write two equations: $W/\lambda = N_1 f_1 \lambda$ and $W/\lambda = N_2 f_2 \lambda$. Therefore, $N_1 f_1 = N_2 f_2$, where suffixes 1, 2 represent the old and revised values respectively of N and f along a particular sight line.

In our data set all of the column densities derived using the COG method are taken from van Steenberg & Shull (1988). Because of the relatively poor resolution and low signal-to-noise of the *IUE*, they derived the column densities by fitting the measured equivalent widths to a single-component COG for the strongest line of the Si II 1525 Å line (with a common b value that is typically based on the seven lines of Fe II). N is then obtained from theoretical single-component COG using the measured equivalent width (by locating the position of the line log (W/λ) on the COG and reading the horizontal value of log ($Nf\lambda$)). The change in the f value will lead to a minor shift in the horizontal axis of the COG with an increase of 14.5% of the f value for the Si II 1525 Å line. Hence, instead of doing an entirely new COG, we have recalculated the N values using the latest f value from NIST. The absorption oscillator strengths (f) and damping constants of the strongest line are used in the calculation of theoretical single-component COG given in their paper. The corrected column densities are listed in Table 1, and the revised oscillator strengths are presented in Table 2. While the maximum correction to the column density was 42%, the more typical correction values were about 20%.

The gas-phase abundance of a species X in the ISM relative to hydrogen is $(N(X)/N(H))_{gas}$, where $N(X)$ and $N(H)(=N(H\,I) + 2N(H_2))$ are the column densities of the species X and hydrogen respectively along a given sight line. Thus, the depletion $\delta(X)$ of a species X relative to hydrogen is (Sofia et al. 1994)

$$\delta(X) = [N(X)/N(H)]_{gas}/[N(X)/N(H)]_{Ref}. \qquad (3)$$

Table 3
The Column Densities of Hydrogen and Calculated Parameters

Star Name	N(H)[a] (cm^{-2})	+Error[a] (cm^{-2})	−Error[a] (cm^{-2})	log n(H)[b]	log $f(H_2)$[c]	$N(Si)_{dust}$[d] (cm^{-2})	+Error (cm^{-2})	−Error (cm^{-2})	D(Si)[e]	+Error	−Error
HD 116658	1.00E+19	2.50E+18	−2.50E+18	−1.37E+00	−5.75E+00	3.21E+14	8.20E+13	8.19E+13	−1.28	0.82	0.82
HD 158926	2.51E+19	6.50E+18	−5.17E+18	−1.33E+00	−6.23E+00	6.95E+14	1.90E+14	1.53E+14	−0.74	0.37	0.33
HD 160578	1.55E+20	3.19E+19	−3.19E+19	−4.70E-01	−5.81E+00	4.33E+15	9.20E+14	9.20E+14	−0.76	0.21	0.21
HD 068273	6.00E+19	6.00E+18	−6.00E+18	−1.13E+00	−5.18E+00	1.02E+15	1.63E+14	1.63E+14	−0.30	0.12	0.12
HD 157246	5.50E+20	8.14E+19	−7.09E+19	−2.91E-01	−1.20E+00	1.72E+16	2.61E+15	2.28E+15	−1.13	0.23	0.18
HD 036486	1.70E+20	3.40E+19	−3.40E+19	−5.86E-01	−5.31E+00	4.57E+15	9.56E+14	9.55E+14	−0.68	0.21	0.21
HD 202904	5.07E+20	1.49E+20	−1.49E+20	−7.85E-02	−1.25E+00	1.60E+16	4.72E+15	4.72E+15	−1.15	0.30	0.30
HD 037043	1.45E+20	1.76E+19	−1.57E+19	−9.39E-01	−5.17E+00	3.39E+15	4.89E+14	4.50E+14	−0.51	0.16	0.15
HD 038771	3.30E+20	3.30E+19	−3.30E+19	−2.68E-01	−4.55E+00	9.64E+15	1.01E+15	1.08E+15	−0.86	0.10	0.26

Notes.
[a] Hydrogen column densities and their errors taken from Gudennavar et al. (2012).
[b] logarithm of $\langle n(H)\rangle$, where $\langle n(H)\rangle = N(H)/d$ as mentioned in the text.
[c] logarithm of $f(H_2)$, where $f(H_2) = 2N(H_2)/[(N(HI) + 2N(H_2)]$.
[d] The column density of silicon in dust, which is calculated using the equation $[N(Si)/N(H)]_{dust} \times N(H)$.
[e] D(Si) and its errors are calculated using the equation mentioned in the text.
(This table is available in its entirety in machine-readable form.)

The logarithmic depletion of the species X, is then

$$D(X) = \log \delta(X) = \log[N(X)/N(H)]_{gas} - \log[N(X)/N(H)]_{Ref}. \quad (4)$$

The dust-phase abundance of a species X relative to hydrogen is

$$[N(X)/N(H)]_{dust} = [N(X)/N(H)]_{Ref} - [N(X)/N(H)]_{gas} \quad (5)$$

where we have adopted the solar abundance of $(Si/H)_{solar} = 33.88$ ppm (Lodders et al. 2009) for $[N(X)/N(H)]_{Ref}$. The column densities of silicon, hydrogen, the derived gas and dust-phase abundances, and depletions for our sample are listed in Table 3. We have recalculated the error bars, where available, with the updated oscillator strengths, and these are also listed in Table 3. We have plotted the depletion of the silicon as a function of the hydrogen density in Figure 2 with 1σ error bars where available. Because the ionization potential of Si I is 8.15 eV and the ionization potential of Si II is 16.35 eV, almost all of the gas-phase silicon associated with the neutral hydrogen regions will be in the form of Si II (Gnacinski & Krogulec 2006).

3. RESULTS & DISCUSSION

We have plotted the depletion of silicon (D(Si)) as a function of the average hydrogen density ($=N(H)/d$, where d is the distance to the star) in Figure 2. There is a clear anticorrelation between the two such that $D(Si) = -0.47\, n(H)$ with a correlation coefficient of −0.86, indicating that sight lines with greater average densities have more dust. Note that we have only used those points with valid errors in the fitting. This may be interpreted using the two phase model of Spitzer (1985) in which the ISM consists of warm clouds with little dust and cold clouds where the grains are both more likely to form through accretion and are better protected from destruction. Those sight lines with higher average densities sample denser clouds and, hence, show greater depletions (Jenkins et al. 1986; Cartledge et al. 2006). There may be cycling of the interstellar silicon between the gas and the dust phases depending on the cloud density (Whittet 2003).

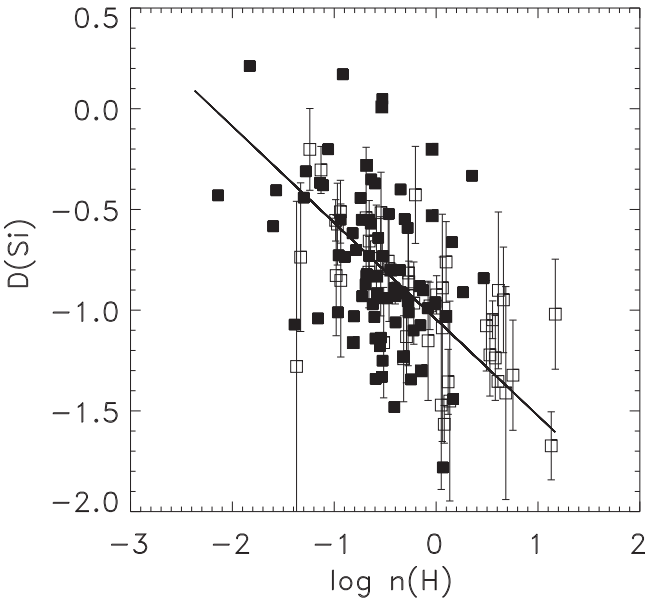

Figure 2. Depletion of Si (D(Si)) plotted as a function of average density of hydrogen along the line of sight (log $\langle n(H)\rangle$) where the reference abundance is taken to be solar. Both the Si abundances and the error bars have been corrected for the updated oscillator strengths. Solid square symbols represent the data points with unusable y-errors; they have not been used in the fitting. The correlation coefficient is $(r) = -0.86$. In subsequent plots we have only shown the data points that have been used in the fitting and for which valid y-errors are available.

A similar effect is seen in Figure 3 where we plot the depletion as a function of $f(H_2)$, the fraction of hydrogen in molecular form, leaving out those points without error bars. There is a break in the data where those sight lines with $f(H_2) < 0.001$ may be identified with diffuse clouds in which the hydrogen is effectively all in the form of atomic gas. For sight lines with $f(H_2) > 0.001$ there is a clear anticorrelation with a correlation coefficient −0.57, while, for $f(H_2) < 0.001$, there is either no or a mild correlation ($r = -0.26$). Self-

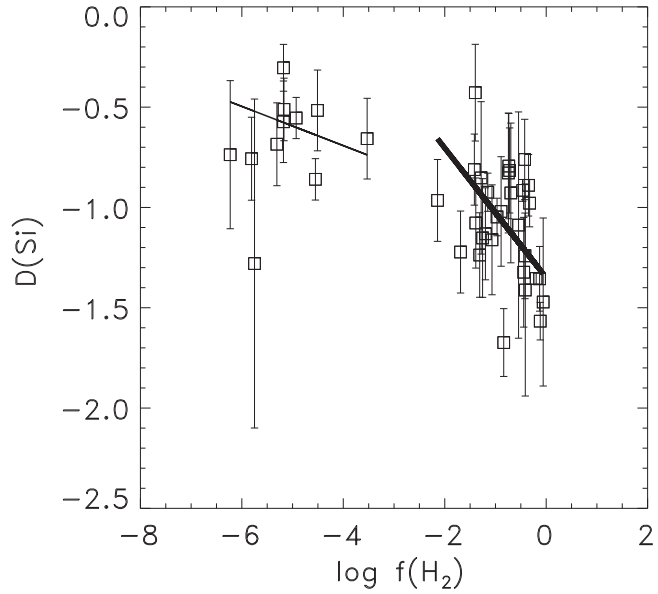

Figure 3. Depletion of Si plotted against the fraction of hydrogen in molecular form (D(Si) vs. log$f$ (H_2)). Associated uncertainties in log $f(H_2)$ and D(Si) are also shown. The thin line and thick line are used to represent the weighted linear least squares fit in the diffuse region and dense region respectively. For $f(H_2) > 0.001$, slope $= -0.32$ and linear correlation coefficient $= -0.57$.

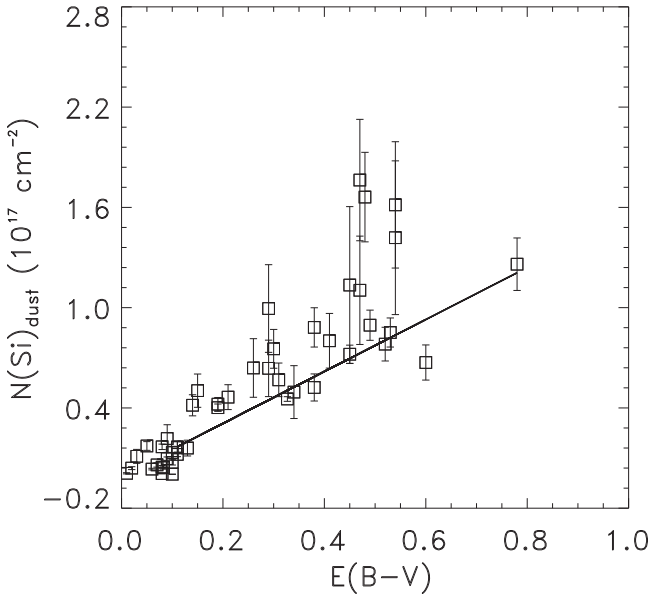

Figure 4. N (Si)$_{\rm dust}$ plotted as a function of $E(B-V)$. Associated uncertainties in $E(B-V)$ and N(Si)$_{\rm dust}$ are also shown. A correlation is found between N(Si)$_{\rm dust}$ and $E(B-V)$ with a correlation coefficient of 0.89 for $E(B-V) > 0.1$. The weighted linear least squares fit to the points is also shown.

shielding becomes important as the amount of molecular hydrogen increases and there is a rapid increase in $f(H_2)$ at the threshold value (Savage & Sembach 1996). The Si depletion is constant with a mean value $D(\mathrm{Si}) = -0.5$ dex for the diffuse clouds while it increases with increasing $f(H_2)$ for the denser clouds, albeit with considerable scatter in both cases. This again suggests that grain growth is favored in dense regions of the ISM (Jones 2000). This study includes measurements from 131 heterogeneous sources, but it confirms most of the previous results (Savage & Bohlin 1979; Harris et al. 1984; see also references in Jensen & Snow 2007a, 2007b, and Jenkins 2009) that find the depletion of Si is correlated with the average hydrogen density along the line of sight ($\langle n(\mathrm{H})\rangle$) as well as the fraction of hydrogen in molecular form $f(H_2)$.

We have plotted the column density of silicon in the dust (N (Si)$_{\rm dust}$) as a function of $E(B-V)$ in Figure 4. There is a strong linear correlation of (N(Si)$_{\rm dust}$) with $E(B-V)$, perhaps with a flattening below $E(B-V) < 0.1$ where there is little dust and most of the silicon may be in the gas phase. Valencic et al. (2004) have measured R_V ($=A_V/E(B-V)$) over 42 of the 131 sight lines, and we have plotted the silicon depletion D(Si) as a function of $1/R_V$ in Figure 5 finding very little correlation ($r = 0.13$, $p < 0.63$). This would be expected if we consider the silicate core–ice mantle model of the dust grain (Li et al. 2007) in which the size of the grain is determined by the size of the core as well as the size of the mantle. Therefore, the grain size will not necessarily vary as a function of the amount of Si going onto dust.

The extinction curve has been parameterized (Table 4) by Fitzpatrick & Massa (1988),

$$\frac{E(\lambda - V)}{E(B-V)} = c_1 + c_2\lambda^{-1} + c_3 D(\lambda^{-1}, \gamma, \lambda_0^{-1}) + c_4 F(\lambda^{-1}) \quad (6)$$

where c_1 and c_2 define the linear background, c_3 and c_4 define the strengths of the 2175 Å bump and the FUV curvature

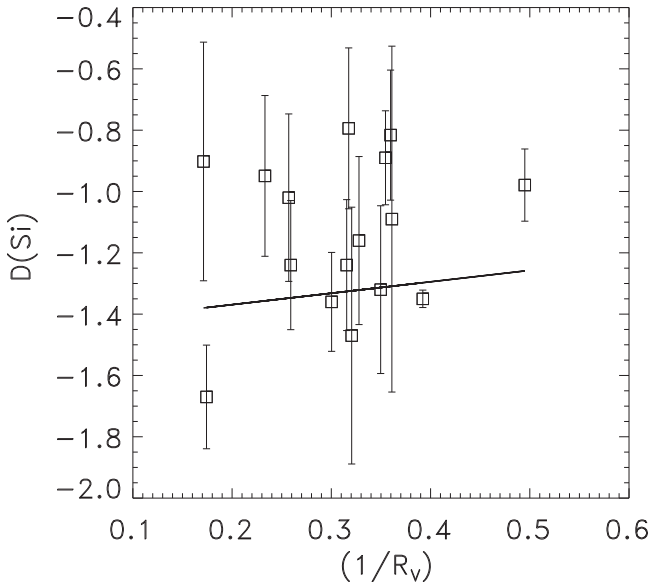

Figure 5. Depletion of Si (D(Si)) plotted as a function of $1/R_V$. Associated uncertainties in $1/R_V$ and D(Si) are also shown. The weighted linear least squares fit to the points is shown. For further explanation please see the text.

respectively, $D(\lambda^{-1}, \gamma, \lambda_0^{-1})$ defines the shape of the bump with γ and λ_0^{-1} representing the FWHM and center of the bump respectively, and $F(\lambda^{-1})$ defines the FUV curvature. These parameters are dependent on $E(B-V)$, and it is more convenient for us to use extinction parameters normalized to A_V by dividing by R_V, where $R_V = A_V/E(B-V)$ as recommended by Cardelli et al. (1989). Valencic et al. (2004) have compiled the extinction parameters for 42 of the sight lines in this paper, and we have plotted the Si depletion as a function of c_1/R_V, c_2/R_V, c_3/R_V, and c_4/R_V, in Figures 6–9, respectively. The correlation coefficients and linear slopes are tabulated in Table 5.

Table 4
Extinction Parameters

Star name	$1/R_V$[a]	±Error	$(c_1/R_V) + 1$[b]	±Error	(c_2/R_V)[b]	±Error	(c_3/R_V)[b]	±Error	(c_4/R_V)[b]	±Error
HD 185418	0.39	0.03	1.82	0.27	0.10	0.02	1.16	0.17	0.16	0.03
HD 023180	0.32	0.04	1.49	0.53	0.10	0.02	1.41	0.29	0.24	0.06
HD 037061	0.23	0.01	1.54	0.15	0.00	0.10	0.31	0.04	0.05	0.01
HD 149038	0.20	0.04	1.18	0.53	0.19	0.05	1.26	0.34	0.14	0.05
HD 203064	0.33	0.04	1.00	0.21	0.25	0.05	0.85	0.24	0.04	0.02
HD 149757	0.39	0.04	1.00	0.10	0.29	0.04	1.87	0.31	0.21	0.05
HD 045314	0.23	0.02	1.07	0.43	0.15	0.02	0.40	0.06	0.05	0.02
HD 069106	0.33	0.05	1.27	0.65	0.10	0.03	0.61	0.19	0.13	0.05
HD 116852	0.41	0.06	0.52	0.25	0.38	0.10	0.63	0.17	0.01	0.01
HD 199579	0.32	0.07	1.10	0.55	0.28	0.07	0.81	0.21	0.20	0.06
HD 024912	0.35	0.06	1.19	0.73	0.27	0.05	0.94	0.22	0.05	0.02
HD 041117	0.32	0.03	1.04	0.33	0.25	0.03	1.37	0.21	0.24	0.04
HD 151804	0.23	0.02	1.40	0.46	0.11	0.02	0.54	0.11	0.12	0.04
HD 147933	0.17	0.01	1.23	0.17	0.02	0.00	0.58	0.09	0.10	0.01
HD 149404	0.28	0.03	1.45	0.31	0.12	0.02	0.80	0.14	0.19	0.04
HD 112244	0.26	0.05	1.46	0.53	0.11	0.03	0.82	0.22	0.19	0.06
HD 209975	0.35	0.05	1.17	0.41	0.26	0.04	1.12	0.22	0.18	0.04
HD 042087	0.32	0.05	1.08	0.68	0.26	0.04	1.41	0.21	0.30	0.05
HD 193322	0.36	0.03	0.91	0.28	0.30	0.04	1.09	0.17	0.03	0.01
HD 002905	0.49	0.16	1.17	0.68	0.42	0.15	1.12	0.41	0.23	0.10
HD 147165	0.26	0.03	1.56	0.30	0.04	0.01	0.63	0.13	0.02	0.01
HD 046056	0.38	0.03	0.76	0.24	0.33	0.04	1.19	0.18	0.20	0.03
HD 154368	0.30	0.01	1.09	0.10	0.22	0.01	1.05	0.10	0.22	0.02
HD 207198	0.36	0.05	0.81	0.26	0.34	0.05	0.98	0.17	0.28	0.04
HD 152233	0.34	0.03	0.54	0.15	0.36	0.05	0.96	0.21	0.10	0.03
HD 152408	0.24	0.02	1.41	0.30	0.10	0.02	0.60	0.11	0.16	0.04
HD 027778	0.39	0.04	1.42	0.25	0.23	0.04	0.88	0.18	0.39	0.06
HD 209339	0.36	0.04	1.16	0.30	0.24	0.04	0.99	0.19	0.08	0.02
HD 101190	0.40	0.03	0.40	0.09	0.40	0.06	1.29	0.23	0.21	0.05
HD 210839	0.50	0.06	0.66	0.39	0.45	0.08	1.55	0.37	0.17	0.05
HD 093205	0.31	0.02	0.93	0.51	0.25	0.03	0.74	0.16	0.17	0.06
HD 122879	0.32	0.03	1.32	0.30	0.23	0.04	1.24	0.23	0.19	0.04
HD 206267	0.35	0.02	1.17	0.36	0.27	0.03	1.02	0.13	0.22	0.04
HD 147888	0.26	0.01	1.47	0.27	0.04	0.01	0.67	0.10	0.09	0.02
HD 001383	0.36	0.02	1.14	0.25	0.23	0.02	1.24	0.17	0.19	0.03
HD 037021	0.17	0.01	1.06	1.05	0.02	0.01	0.23	0.04	0.01	0.01
HD 030614	0.33	0.04	1.10	0.29	0.20	0.03	0.75	0.15	0.13	0.03
HD 152236	0.27	0.03	0.76	0.66	0.26	0.05	1.29	0.37	0.15	0.03
HD 303308	0.33	0.02	0.87	0.21	0.26	0.03	0.90	0.13	0.16	0.03
HD 093843	0.26	0.03	1.37	0.50	0.15	0.04	0.45	0.11	0.18	0.06
HD 034078	0.29	0.02	1.37	0.20	0.14	0.02	1.22	0.16	0.18	0.02
HD 046202	0.34	0.03	0.83	0.26	0.28	0.03	1.07	0.16	0.17	0.03

Notes.
[a] Where $R_V = A_V/E(B-V)$, the ratio of total to selective extinction.
[b] Where c_1/R_V, c_2/R_V, c_3/R_V, and c_4/R_V are the Fitzpatrick & Massa (1988) parameters for the intercept, slope, 2175 Å bump strength, and the strength of the non-linear FUV rise of the extinction curve, respectively.
Reference. (1) Valencic et al. (2004).

We find that the Si depletion is not correlated with either (c_1/R_V) or (c_2/R_V), suggesting that the linear part of the extinction curve is independent of the Si depletion. The depletion increases slowly with the bump strength (c_3/R_V) and with the FUV curvature (c_4/R_V), suggesting that silicon plays a small but significant role in both the 2175 Å bump and in the FUV rise. Figure 8 contains information about bump strength. It is interesting that the most depleted sight lines have a higher bump strength (c_3) and/or a low R_V. The low R_V sight lines comprise a larger fraction of small grains than high R_V sight lines (Valencic et al. 2004). This indicates that for the high depletion sight lines there is an increase in the fraction of small grains and vice versa. Hence, as the strength of the extinction bump increases and/or the fraction of small grains increases (low R_V), most of the silicon is depleted from the gas phase onto dust grains.

Figure 9 shows the correlation between Si depletion and FUV curvature, which indicates the presence of small grains in the ISM. This is consistent with previous studies that find silicate grains are responsible for the FUV rise (Mathis et al. 1977; Hong & Greenberg 1980; Draine & Lee 1984; Weingartner & Draine 2001), although, some studies suggest graphite or PAHs (Polyaromatic Hydrocarbons) (Léger et al. 1989; Jenniskens et al. 1992; Désert et al. 1995; Li & Greenberg 1997) as the possible reasons for the 2175 Å bump feature and FUV rise. A gradual increase in FUV extinction with an increase in density indicates either the incorporation of depleted Si into a new population of small grains or the

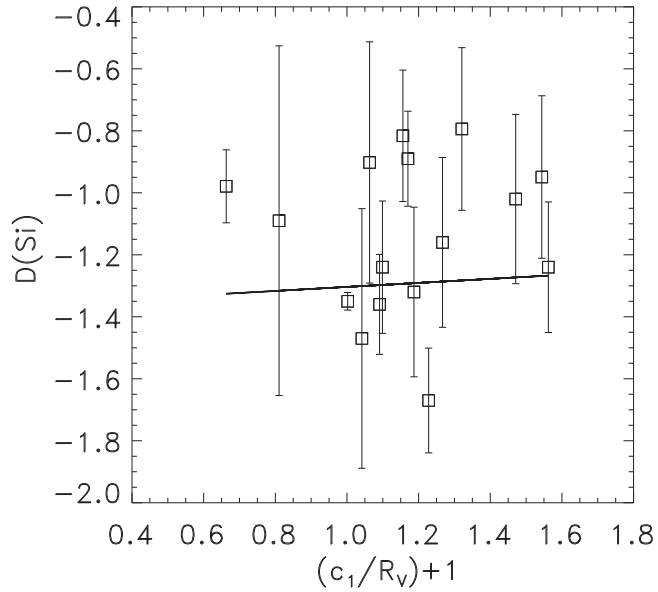

Figure 6. Depletion of Si (D(Si)) plotted as a function of $(c_1/R_V) + 1.0$. Associated uncertainties in $(c_1/R_V) + 1.0$ and D(Si) are also shown. The weighted linear least squares fit to the points is shown.

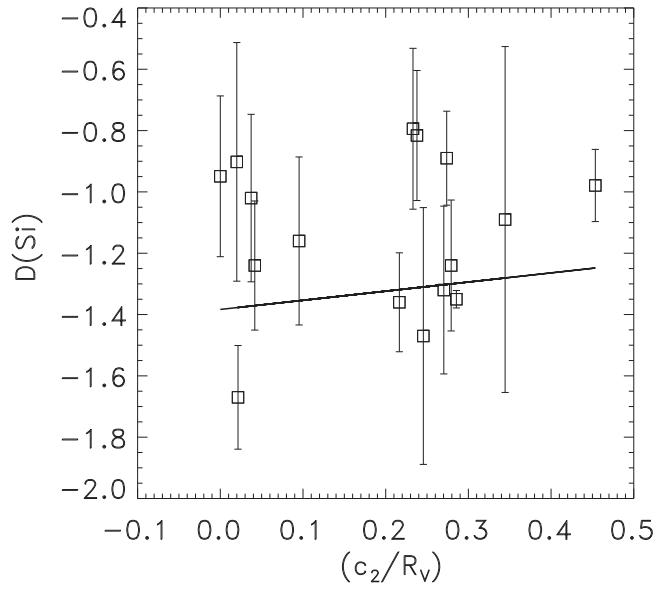

Figure 7. Depletion of Si (D(Si)) plotted as a function of c_2/R_V. Associated uncertainties in c_2/R_V and D(Si) are also shown. The weighted linear least squares fit to the points is also shown.

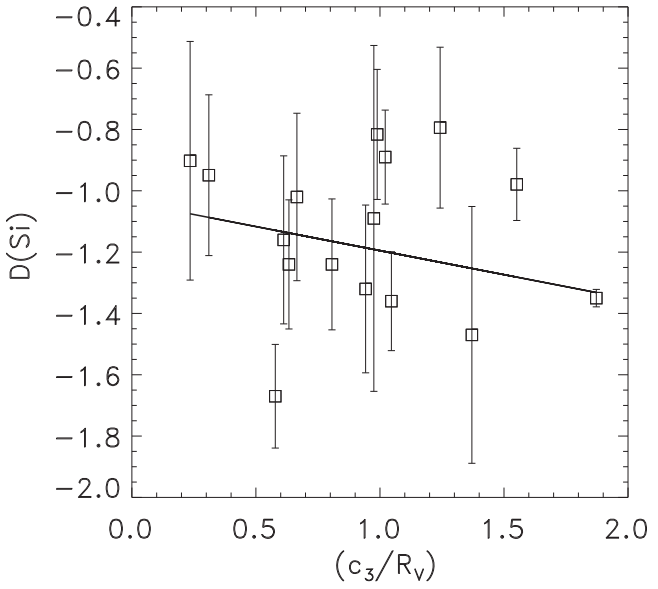

Figure 8. Depletion of Si (D(Si)) plotted as a function of c_3/R_V. Associated uncertainties in c_3/R_V and D(Si) are also shown. The weighted linear least squares fit to the points is shown.

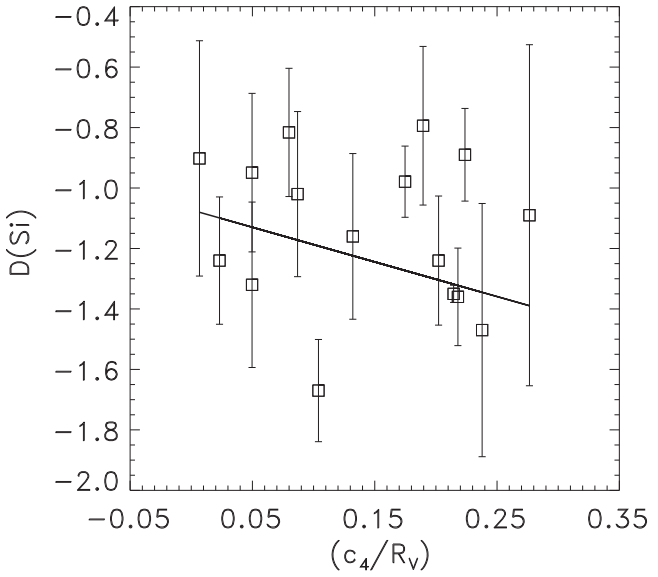

Figure 9. Depletion of Si (D(Si)) plotted as a function of c_4/R_V. Associated uncertainties in c_4/R_V and D(Si) are also shown. The weighted linear least squares fit to the points is shown.

survival of smaller grains in denser environments. The smaller grains, like nano silicate grains, may also contribute to the FUV rise. Their effect on depletion is not significant since they account for only about 5% of total interstellar silicon (Li & Mann 2012). Hence, the grains that account for the linear extinction slope and the FUV curvature may belong to two different populations (Fitzpatrick & Massa 1988).

We could reproduce the Miller et al. (2007) plot showing a correlation between the dust-phase abundance of silicon and c_4, but it would have a low correlation coefficient ($r = 0.30$, $p < 0.24$) (Figure 10). The sample we used is larger than the six sight lines used by Miller et al. (2007). The c_4 is a parameter that defines the strength of the FUV curvature of the extinction curve, and it can be used as representative for the population of small grains. Thus, we suggest that silicon depletion is showing a small but significant correlation with the small grain populations along these sight lines. A larger sample of high-quality measurements of silicon and hydrogen column density should give us a better understanding of the relation between the dust-phase silicon abundance and the ultraviolet extinction parameters.

4. SUMMARY

In this study, we have investigated Si abundances along 131 lines of sight from archival observations (Gudennavar et al. 2012). These include absorption line measurements of Si II at wavelengths of 1020.699 Å, 1190.4158 Å, 1193.2897 Å, 1260.4221 Å, 1304.3702 Å, 1526.7066 Å, 1808.0126 Å, and

Table 5
Fit Parameters

Figures[a]	Relation	Correlation	Slope Coefficient
Figure 6	$(c_1/R_V) + 1$ and D(Si)	0.06 ($p < 0.82$)	0.06
Figure 7	(c_2/R_V) and D(Si)	0.15 ($p < 0.58$)	0.29
Figure 8	(c_3/R_V) and D(Si)	−0.42 ($p < 0.10$)	−0.17
Figure 9	(c_4/R_V) and D(Si)	−0.32 ($p < 0.23$)	−1.14

Note.
[a] Correlation coefficients with significance values in brackets and linear slopes for Figures 6–9, respectively.

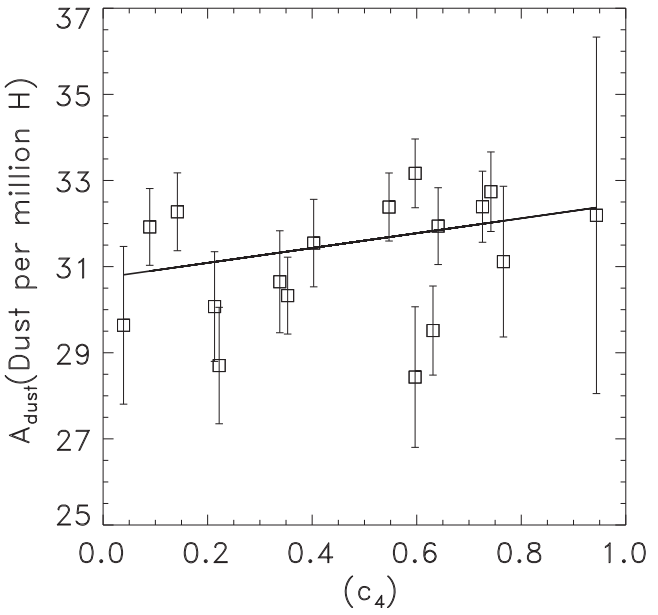

Figure 10. Number of silicon atoms in the dust per 10^6 H, $(A(\mathrm{Si})_{\mathrm{dust}})$ as a function of the Fitzpatrick & Massa (1988) extinction coefficient c_4. Associated uncertainties in D(Si) are also shown. The weighted linear least squares fit to the points is shown.

2334.605 Å. The derived oscillator strength of each of these lines has changed over the years of observations, and we have corrected all to the latest National Institute of Standards and Technology (NIST) values (Kelleher & Podobedova 2008), leading to corrections of up to 42% from the previously reported column densities.

We find that the Si depletion increases with the average hydrogen density, indicating that more of the silicon is tied up in interstellar dust grains in dense clouds. The depletion of silicon is constant when there is little molecular hydrogen but increases when the molecular hydrogen fraction ($f(\mathrm{H_2})$) is greater than 0.001, which is characteristic of dense clouds with self-shielding of the H_2. We find that the Si depletion is not correlated with either the (c_1/R_V) or with the (c_2/R_V), suggesting that the linear part of the extinction curve is independent of the Si depletion. The Si depletion increases slowly with the bump strength (c_3/R_V) and with the FUV curvature (c_4/R_V), suggesting that silicon plays a small but significant role in both the 2175 Å bump and in the FUV rise. This is consistent with Miller et al. (2007) who found the FUV rise was correlated with the dust-phase abundance of silicon, using a limited sample of only six sight lines.

Silicates are an important component in almost every grain model for the ISM, from the MRN model (Mathis et al. 1977) to present models (Clayton et al. 2003). Our results fit well with the silicon core—ice mantle model of Li et al. (2007), in which the size of the grain is determined by the size of the core as well as the size of the mantle. A correlation between Si depletion and the FUV curvature, however, is a strong indication that silicates do contribute significantly to this feature.

We acknowledge financial support by the Science & Engineering Research Board, Department of Science and Technology (DST), Ministry of Science and Technology, Government of India, New Delhi, India under the grant No. SR/S2/HEP-50/2012.

REFERENCES

Cardelli, J., Clayton, G., & Mathis, J. 1989, ApJ, 345, 245
Cartledge, S. I. B., Lauroesch, J. T., Meyer, D. M., & Sofia, U. J. 2006, ApJ, 641, 327
Clayton, G. C., Wolff, M. J., Sofia, U. J., Gordon, K. D., & Misselt, K. A. 2003, ApJ, 588, 871
Désert, F.-X., Jenniskens, P., & Dennefeld, M. 1995, A&A, 303, 223
Draine, B. T., & Lee, H. M. 1984, ApJ, 285, 89
Fitzpatrick, E. L., & Massa, D. 1988, ApJ, 328, 734
Gnacinski, P., & Krogulec, M. 2006, AcA, 56, 373
Gudennavar, S. B., Bubbly, S. G., Preethi, K., & Jayant, M. 2012, ApJS, 199, 8
Harris, A. W., Gry, C., & Bromage, G. E. 1984, ApJ, 284, 157
Henning, Th. 2010, ARA&A, 48, 21
Hong, S. S., & Greenberg, J. M. 1980, A&A, 88, 194
Jenkins, E. B. 2009, ApJ, 700, 1299
Jenkins, E. B., Savage, B. D., & Spitzer, L., Jr. 1986, ApJ, 301, 355
Jenniskens, P., Ehrenfreund, P., & Désert, F.-X. 1992, A&A, 265, L1
Jensen, A. G., & Snow, T. P. 2007a, ApJ, 669, 378
Jensen, A. G., & Snow, T. P. 2007b, ApJ, 669, 401
Jones, A. P. 2000, JGR, 105, 10257
Kelleher, D. E., & Podobedova, L. I. 2008, JPCRD, 37, 1285
Léger, A., Verstraete, L., D'Hendecourt, L., et al. 1989, in IAU Symp. 135, Interstellar Dust, ed. L. J. Allamandola, & A. G. G. M. Tielens (Kluwer, Dordrecht), 173
Li, A., & Greenberg, J. M. 1997, A&A, 323, 566
Li, A., & Mann, I. , 2012, ASSL, 385, 5
Li, M. P., Zhao, G., & Li, A. 2007, MNRAS, 382, 26
Lodders, K., Palme, H., & Gail, H. P. 2009, in Abundances of the Elements in the Solar System, Vol. VI/4B, ed. J. E. Trümper (Berlin, Heidelberg, New York: Springer), 560
Mathis, J. S., Rumpl, W., & Nordsieck, K. H. 1977, ApJ, 217, 425
Miller, A., Lauroesch, J. T., Sofia, U. J., Cartledge, S. I. B., & Meyer, D. M. 2007, ApJ, 659, 441
Redfield, S., & Linsky, J. L. 2004, ApJ, 602, 776
Savage, B. D., & Bohlin, R. C. 1979, ApJ, 229, 136
Savage, B. D., & Sembach, K. R. 1996, ARA&A, 34, 279
Sofia, U. J., Cardelli, J. A., & Savage, B. D. 1994, ApJ, 430, 650
Sonnentrucker, P., Friedman, S. D., Welty, D. E., York, D. G., & Snow, T. P. 2003, ApJ, 596, 350
Spitzer, L. 1985, ApJL, 290, L21
Spitzer, L., & Fitzpatrick, E. L. 1995, ApJ, 445, 196
Tielens, A. G. G. M. 2005, Physics and Chemistry of the Interstellar Medium (Cambridge: Cambridge Univ. Press)
Valencic, L. A., Clayton, G. C., & Gordon, K. D. 2004, ApJ, 616, 912
van Steenberg, M. E., & Shull, J. M. 1988, ApJS, 67, 225
Weingartner, J. C., & Draine, B. T. 2001, ApJ, 548, 296
Whittet, D. C. B. 2003, Dust in the Galactic Environment (2nd ed.; Bristol: Institute of Physics Publishing)